Check for updates

Received: 30 November 2022 | Revised: 6 March 2023 | Accepted: 10 March 2023

DOI: 10.1002/pro.4624

FOR THE RECORD

THE PROTEIN SOCIETY WILEY

A splicing variant of EDS1 from *Vitis vinifera* forms homodimers but no heterodimers with PAD4

Martin Voss[1] | **Leland J. Cseke**[2] | **Walter Gassmann**[2] | **Karsten Niefind**[1]

[1]Department für Chemie, Institut für Biochemie, Universität zu Köln, Köln, Germany

[2]Division of Plant Science and Technology, Interdisciplinary Plant Group, CS Bond Life Sciences Center, University of Missouri, Columbia, Missouri, USA

Correspondence
Karsten Niefind, Department für Chemie, Institut für Biochemie, Universität zu Köln, Zülpicher Straße 47, D-50674 Köln, Germany.
Email: karsten.niefind@uni-koeln.de

Funding information
Deutsche Forschungsgemeinschaft, Grant/Award Number: NI 643/6-1

Review Editor: John Kuriyan

Abstract

Enhanced Disease Susceptibility 1 (EDS1), a key component of microbe-triggered immunity and effector-triggered immunity in most higher plants, forms functional heterodimeric complexes with its homologs Phytoalexin Deficient 4 (PAD4) or Senescence-associated Gene 101 (SAG101). Here, the crystal structure of VvEDS1^{Nterm}, the N-terminal domain of EDS1 from *Vitis vinifera*, is reported, representing the first structure of an EDS1 entity beyond the model plant *Arabidopsis thaliana*. VvEDS1^{Nterm} has an α/β-hydrolase fold, is similar to the N-terminal domain of *A. thaliana* EDS1 and forms stable homodimers in solution as well as in crystals. These VvEDS1^{Nterm} homodimers are spatially incompatible with heterodimers with PAD4 or SAG101, they explain why VvEDS1^{Nterm} does not interact with *V. vinifera* PAD4 according to gel filtration, and they serve as a guide to develop a plausible, albeit experimentally not verified model of full-length EDS1. VvEDS1^{Nterm} is a splicing variant comprising two of three exons of the *VvEDS1* gene. It originates from a naturally occurring mRNA, in which the first of two introns was removed while the second one containing a stop codon close to the exon/intron border was retained. This is a potential case of intron retention and the first report of this phenomenon in the context of EDS1. Its biological significance has not yet been clarified, nor has the question if a VvEDS1^{Nterm} protein with a specific function can occur under physiological conditions.

KEYWORDS

alternative splicing, EDS1 homodimerization, enhanced disease susceptibility 1, intron retention, phytoalexin deficient 4, plant innate immune system, *Vitis vinifera*

1 | INTRODUCTION

Erysiphe necator is an obligate biotrophic fungus that causes the plant infectious disease powdery mildew in *Vitis vinifera*, the most frequently cultivated species of grapevine (Qiu et al., 2015). The parasite originates in North America, but after its unintentional transfer to Europe in the 19th century, it spread to viticultural regions worldwide. *V. vinifera* has a Eurasian origin and cultivation history (Magris et al., 2021) and is therefore highly susceptible to *E. necator* since it could not acquire specific defense mechanisms against the pathogen during evolution. In contrast, wild North American grape species like *V. rotundifolia* or *V. aestivalis* are significantly

This is an open access article under the terms of the Creative Commons Attribution-NonCommercial License, which permits use, distribution and reproduction in any medium, provided the original work is properly cited and is not used for commercial purposes.
© 2023 The Authors. *Protein Science* published by Wiley Periodicals LLC on behalf of The Protein Society.

more resistant against *E. necator* infections. These observations inspired expression studies to reveal and characterize genetic and molecular components of powdery mildew defense in wild and cultivated *Vitis* species (Chong et al., 2008; Fung et al., 2008; Gao et al., 2010; Gao et al., 2014).

One of the identified resistance genes was *ENHANCED DISEASE SUSCEPTIBILITY 1* (*EDS1*) which is differentially expressed in *Vitis* species and derived cultivars correlating with their susceptibility to powdery mildew (Gao et al., 2010). At the time of these observations, an *EDS1* ortholog in *Arabidopsis thaliana* and its product, the protein AtEDS1, were already well known as key factors of plant innate immunity (Falk et al., 1999; Parker et al., 1996; Wiermer et al., 2005). AtEDS1 has been characterized to be a monomeric protein (Voss et al., 2019), but for its signaling functions it recruits interaction partners and forms heterodimeric and mutually exclusive complexes (Huang et al., 2022; Wagner et al., 2013) with two paralogous proteins, either with AtPAD4—product of the gene *PHYTOALEXIN DEFICIENT 4* (Feys et al., 2001; Jirage et al., 1999)—or with AtSAG101—product of *SENESCENCE-ASSOCIATED GENE 101* (Feys et al., 2005; He & Gan, 2002). The resulting complexes AtEDS1/AtPAD4 and AtEDS1/AtSAG101 recognize and coordinate specific second messenger molecules, which are synthesized from ATP and NAD^+ under the catalysis of activated TIR-domain containing immune receptor proteins (Huang et al., 2022; Jia et al., 2022), as a prerequisite of subsequent binding of the helper NLR proteins ADR1 or NRG1 (Pruitt et al., 2021; Sun et al., 2021).

In planta complementation experiments with *Arabidopsis* knockout lines demonstrated that VvEDS1, which shares a sequence identity of 43.4% with AtEDS1 (Gao et al., 2014), can functionally substitute the latter (Gao et al., 2010). Consistent to this, VvEDS1 physically interacts *in planta* with AtPAD4 and also with VvPAD4, the *V. vinifera* ortholog of AtPAD4, according to bimolecular fluorescence complementation studies (Gao et al., 2014). However, VvPAD4 for its part is neither able to functionally complement AtPAD4 *in planta* nor does it interact with AtEDS1 (Gao et al., 2014).

Thus, among all similarities, subtle differences of EDS1 protein family members between *V. vinifera* and *A. thaliana* exist. To elucidate the structural background of these features, we started efforts to solve the crystal structure of VvEDS1. In this context, we discovered a complementary DNA (cDNA) resulting potentially from intron retention, the most frequent form of alternative splicing of pre-mRNA in plants (Kufel et al., 2022), and coding for a VvEDS1 variant significantly smaller than the wildtype protein. This shortened VvEDS1 variant is the main subject of the study presented here.

2 | RESULTS AND DISCUSSION

2.1 | VvEDS1^{Nterm} is the result of intron retention

VvEDS1 is a gene with three exons and two introns and has the identifier 100233033 in the NCBI Gene database (Brown et al., 2015). The corresponding entry of GenBank (Sayers et al., 2022) is JF436934.1; its translation product is a protein with 596 amino acids and with identifier G3F1Q6 in UNIPROT (UniProt Consortium, 2021).

In an analysis of the expression of *EDS1*-like genes in the *V. vinifera* cultivar "Cabernet Sauvignon", we discovered a cDNA significantly longer than expected. The sequence of this cDNA shows that the first intron of the *VvEDS1* gene had been fully removed during pre-mRNA splicing while the second one was retained. This intron contains the stop codon TGA from position 22 to 24 in frame with the preceding exon (Figure 1a). As a consequence, the third exon is excluded from the coding sequence which spans over just 1089 nucleotides. The protein to be expected from this CDS comprises the first 355 residues of full-length VvEDS1 plus 7 residues translated from the beginning of intron 2 (Figure 1b). We refer to this protein as VvEDS1^{Nterm} from here on, because it includes most of the N-terminal domain of VvEDS1—a Lipase_3 domain according to PFAM (Mistry et al., 2021) with an α/β-hydrolase fold (Wagner et al., 2013)—while the C-terminal EP domain was left out.

We validated the presence of the VvEDS1^{Nterm} encoding mRNA in the analyzed *V. vinifera* sample. It contains a long 3′-untranslated region (3′-UTR) (Figure 1a), and mRNAs of this kind—meaning with an 3′-UTR longer than 350 nt as reported for *Arabidopsis* (Kalyna et al., 2012)—should normally be sensitive to nonsense-mediated decay (NMD) (Lykke-Andersen & Jensen, 2015). The persistence of the VvEDS1^{Nterm} encoding mRNA could indicate that the NMD pathway was down-regulated as it is possible for instance for *Arabidopsis* after infection with *Pseudomonas syringae* (Gloggnitzer et al., 2014). Alternative splicing and especially intron retention are major phenomena in plants (Chaudhary et al., 2019), but to our knowledge, they were never reported for EDS1. Therefore, it needs experimental clarification whether the occurrence of this VvEDS1^{Nterm} encoding mRNA represents a genuine case of intron retention and is associated with a specific role (Wong & Schmitz, 2022).

1469896x, 2023, 4, Downloaded from https://onlinelibrary.wiley.com/doi/10.1002/pro.4624 by Bibl. der Universitat zu Koln, Wiley Online Library on [23/11/2026]. See the Terms and Conditions (https://onlinelibrary.wiley.com/terms-and-conditions) on Wiley Online Library for rules of use; OA articles are governed by the applicable Creative Commons License

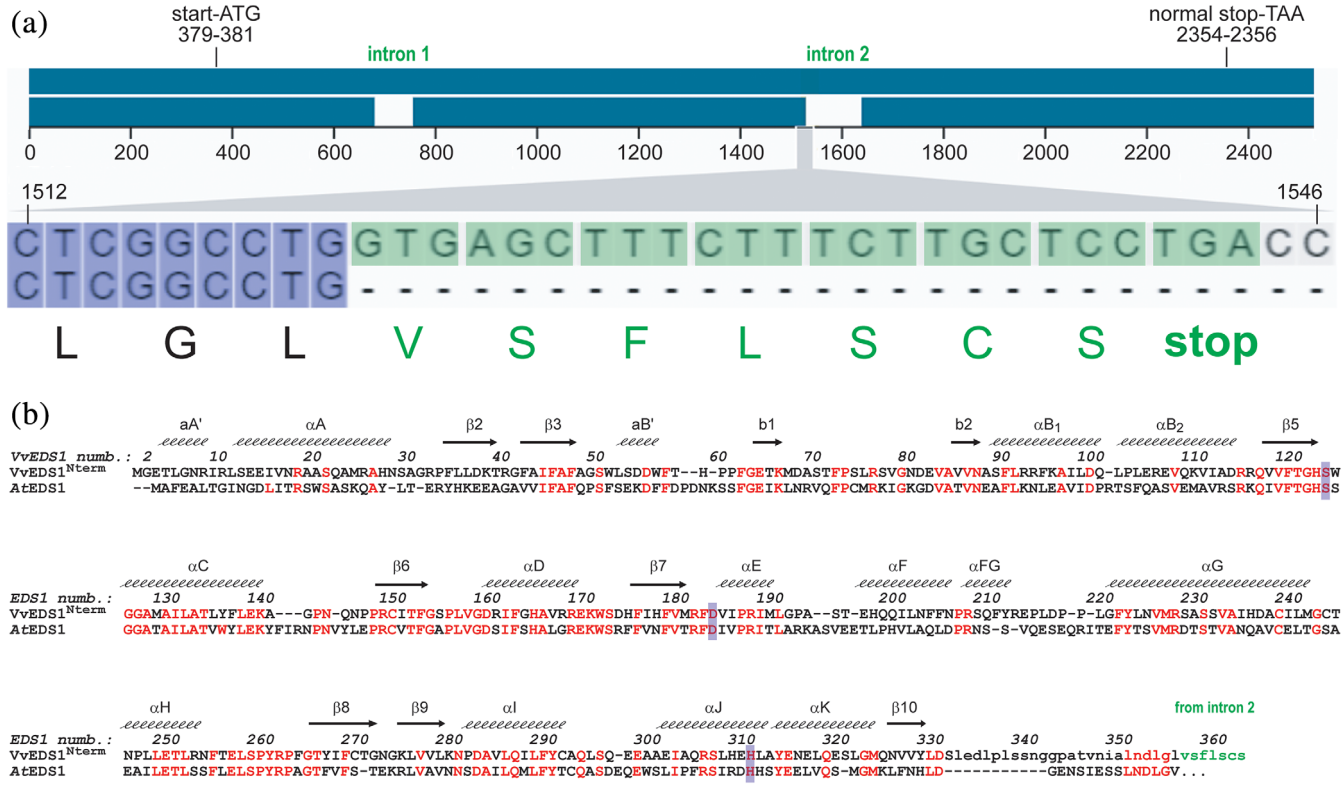

FIGURE 1 Sequence overview of VvEDS1^{Nterm}. (a) Condensed alignment of the nucleotide sequences of the *Vitis vinifera EDS1* gene and of the coding region of the bona fide mRNA transcript (entry JF436934.1 in GenBank; Sayers et al., 2022) in order to illustrate the position of the two introns. The start of intron 2, which is translated as novel C-terminal tail of VvEDS1^{Nterm}, was zoomed for illustration. (b) Structure-based sequence alignment of VvEDS1^{Nterm} and the N-terminal domain of AtEDS1 calculated with TM-align (Zhang & Skolnick, 2005) using PDB_ID 8B28 (VvEDS1^{Nterm}, this work) and PDB_ID 4NFU (AtEDS1/AtSAG101 complex; Wagner et al., 2013). In the C-terminal part of VvEDS1^{Nterm} and the beginning of intron 2 (green), the sequence was printed with lowercase letters because this region is structurally disordered. Conserved positions are printed in red. The residues of the SHD-triad are highlighted in purple. The established designation of EDS1 secondary structure elements follows previous determinations (Voss et al., 2019; Wagner et al., 2013); it differs slightly from the classical scheme for α/β-hydrolase fold domains (Ollis et al., 1992) as explained by Wagner (2013).

In particular, the question whether the translation product VvEDS1^{Nterm} is actually synthesized *in vivo* under certain conditions and if so, whether it exerts a physiological function—for instance, by interaction with the interaction partners described for full-length VvEDS1 including VvEDS1 itself (Gao et al., 2014)—is open. What speaks in favor of such an option is the fact that VvEDS1^{Nterm} to a large extent comprises a folding domain and is a stable protein, as the *in vitro* studies described below demonstrate.

2.2 | VvEDS1^{Nterm} forms homodimers in solution, but no heterodimers with VvPAD4

VvEDS1^{Nterm} and VvPAD4 were bacterially expressed and subsequently purified, while efforts to prepare full-length VvEDS1 were not successful so far. We applied both proteins alone and a 1:1 mixture of them to a calibrated analytical gel filtration column in order to determine native molecular masses of the isolated proteins and of a potential complex of them.

All three chromatograms showed a single peak corresponding to a molecular weight in the range of 65 kDa (Figure 2). The apparent molecular weight of a protein from gel filtration depends both on its size and its shape and does therefore not allow an unequivocal conclusion on its quaternary structure, but with this restriction, the gel filtration results fits reasonably well to a VvPAD4 monomer (calculated mass: 66.9 kDa), and to a dimeric state of VvEDS1^{Nterm} (calculated mass: 81.0 kDa). In contrast, AtEDS1$^{1-384}$, the N-terminal domain of *A. thaliana* EDS1, is mainly monomeric, however with a tendency to form homodimers as well (Wagner, 2013). Remarkably, the chromatogram of the VvEDS1^{Nterm}/VvPAD4 mixture

1469896x, 2023, 4, Downloaded from https://onlinelibrary.wiley.com/doi/10.1002/pro.4624 by Bibl. der Universitat zu Koln, Wiley Online Library on [23/11/2026]. See the Terms and Conditions (https://onlinelibrary.wiley.com/terms-and-conditions) on Wiley Online Library for rules of use; OA articles are governed by the applicable Creative Commons License

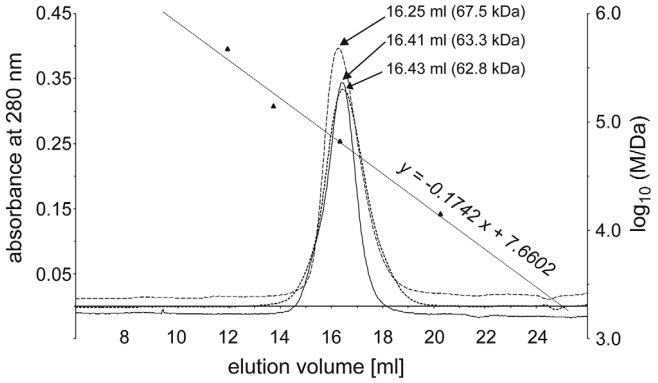

FIGURE 2 Overlaid analytical gel filtration chromatograms of VvEDS1^{Nterm} (long-dashed line), VvPAD4 (solid line) and a 1:1-mixture of both (short-dashed line). The column was calibrated with four standard proteins represented by black triangles; their logarithmic molecular masses (secondary vertical axis) were plotted against the elution volume.

does not show any peak shift toward a higher molecular weight. Thus, VvEDS1^{Nterm} does not form a complex with VvPAD4 in contrast to full-length VvEDS1 (Gao et al., 2014).

2.3 | Crystal structure of VvEDS1^{Nterm}

Crystallization experiments were performed with VvPAD4 and VvEDS1^{Nterm}, but they were successful only in the case of the latter for which a crystal structure with a resolution higher than 2 Å was determined (Table 1).

In a global 3D-fit on the EDS1-part of the nonactivated AtEDS1/AtSAG101 complex (PDB_ID 4NFU; Wagner et al., 2013), VvEDS1^{Nterm} aligns with 300 of its 331 C_α-atoms (RMSD: 1.51 Å). If an AtEDS1/AtPAD4 complex—either nonactivated (PDB_ID 7XDD; Huang et al., 2022) or activated with phosphoribosyl-ADP (PDB_ID 7XEY; Huang et al., 2022)—is used for the comparison, the corresponding values are 293 C_α-atoms and an RMSD of 1.43 Å (nonactivated case) or 298 C_α-atoms and an RMSD of 1.62 Å (activated case). Thus, VvEDS1$^{N\text{-}term}$ and the N-terminal domains of AtEDS1 are structurally fairly similar (Figure 3a) independent of the AtEDS1 binding partner and activation state of the complex. This global view is confirmed by a more detailed inspection: for example, both AtEDS1 and VvEDS1^{Nterm} show the classical elements of an α/β-hydrolase fold, among them a topology composed of a central open and predominantly parallel β-sheet with two layers of α-helices attached to the sides (Figure 3a) and a potentially catalytic SHD-triad with the succession Ser, Asp and His in the primary sequence (Figure 1b) (Ollis et al., 1992). Furthermore, VvEDS1^{Nterm} has all deviations from and supplementations to the canonical α/β-hydrolase fold topology known from AtEDS1 (Voss et al., 2019; Wagner et al., 2013): (i) in the first half of the central β-sheet, two strands—β1 and β4—are missing; (ii) conversely, the second half of the canonical β-sheet is enlarged by two

TABLE 1 X-ray diffraction data and refinement statistics of the VvEDS1^{Nterm} crystals.

PDB code	8B28
X-ray diffraction data quality	
Wavelength	0.91508
Synchrotron (beamline)	ESRF (ID30B)
Space group	C2
Cell dimensions	
a, *b*, *c* (Å)	144.55, 65.01, 45.45
α, *β*, *γ* (°)	90.00, 105.48, 90.00
Resolution (Å) (highest shell)	43.81–1.76 (1.94–1.76)[a]
R_{sym} (%)	10.6 (66.8)[a]
CC1/2	0.988 (0.658)[a]
Signal-to-noise ratio (I/σ_I)	5.7 (1.4)[a]
No. of unique reflections	29,029 (1451)[a]
Completeness (spherical) (%)	71.3 (13.7)[a]
Completeness (ellipsoidal) (%)[b]	88.2 (47.9)[a]
Multiplicity	2.8 (2.9)[a]
Wilson-plot B factor (Å^2)	22.36
Refinement and structure quality	
No. of reflections for R_{work}/R_{free}	28,010/1010
R_{work}/R_{free} (%)	17.4/20.6
No. of protomers per AU	2
No. of non-H-atoms	2963
Protein	2662
Ligand/ion	32
Water	269
Average B factors (Å^2)	30.38
Protein	29.68
Ligand/ion	40.93
Water	36.07
RMS deviations	
Bond lengths (Å)	0.003
Bond angles (°)	0.57
Ramachandran plot	
Favored (%)	97.57
Allowed (%)	2.43
Outliers (%)	0.00

[a]The values in brackets refer to the highest resolution shell.
[b]After anisotropic analysis with STARANISO (Tickle et al., 2018).

1469896x, 2023, 4, Downloaded from https://onlinelibrary.wiley.com/doi/10.1002/pro.4624 by Bibl. der Universitat zu Koln, Wiley Online Library on [23/11/2026]. See the Terms and Conditions (https://onlinelibrary.wiley.com/terms-and-conditions) on Wiley Online Library for rules of use; OA articles are governed by the applicable Creative Commons License

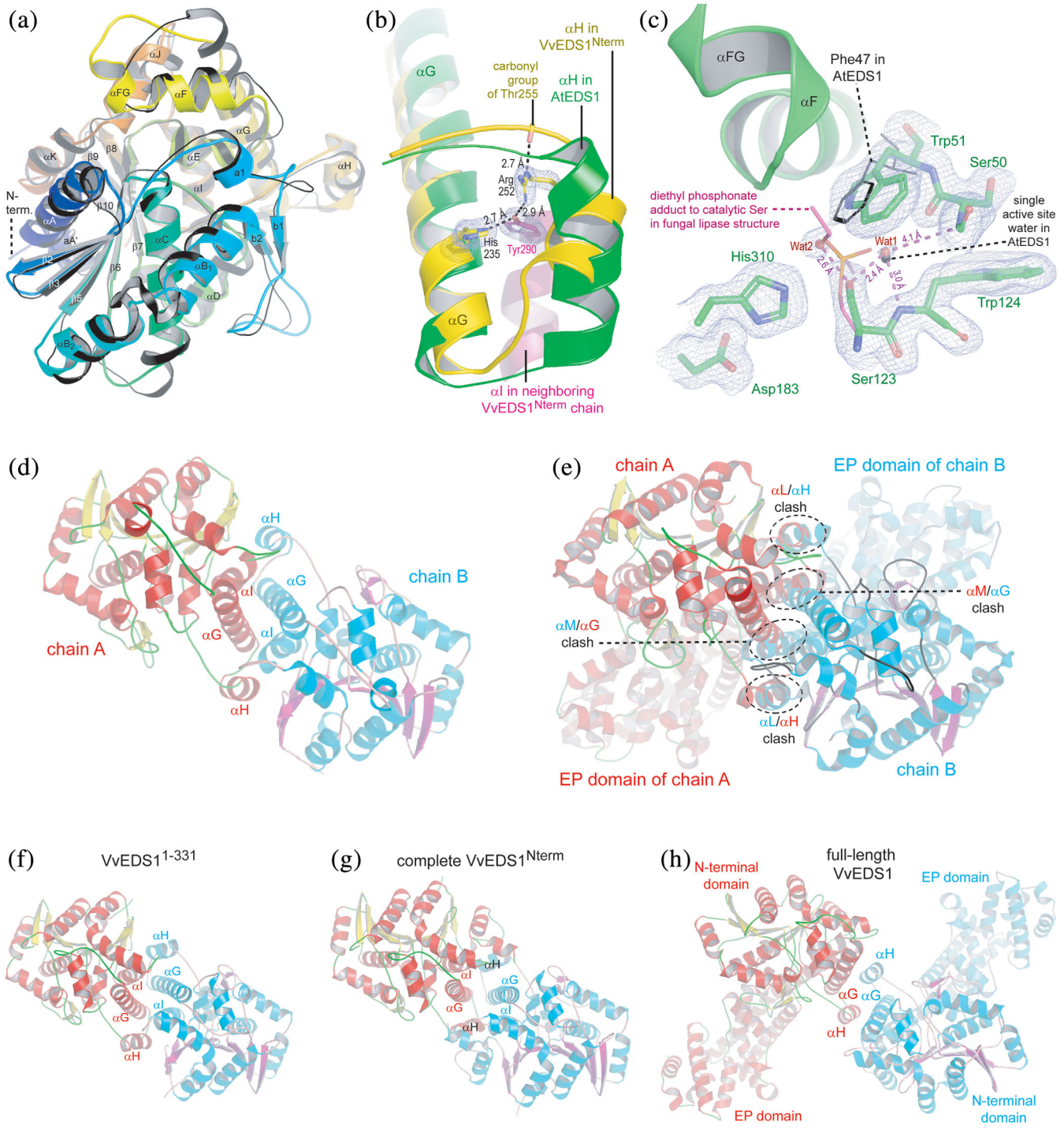

FIGURE 3 Crystal structure and structural comparisons of VvEDS1^{Nterm}. (a) Overview of the VvEDS1^{Nterm} monomer structure; for comparison, the equivalent part of AtEDS1 (PDB_ID 4NFU; Wagner et al., 2013) was drawn in black. (b) Comparison of the αG/αH region in the VvEDS1^{Nterm} homodimer (chain 1: yellow; chain 2: magenta) and AtEDS1 (green; PDB_ID 4NFU; Wagner et al., 2013) after structural overlay of the whole proteins; three interface side chains, connected by hydrogen bonds (dotted black lines), are drawn covered by ($2F_o - F_c$) electron density (contouring level 1.5σ). (c) The potentially catalytic SHD-triad of VvEDS1^{Nterm} with its nearest environment embedded in final ($2F_o - F_c$) electron density (contouring level 1.0σ). For comparison, parts of AtEDS1 from PDB_ID 4NFU (Wagner et al., 2013) (black C-atoms) and of a bacterial lipase with a covalently modified catalytic serine from PDB_ID 4TGL (Derewenda et al., 1992) (magenta-colored C-atoms) are drawn. (d) Experimental structure of a VvEDS1^{Nterm} homodimer with helical interface composed of αG, αH, and αI. (e) *In silico* model of an AtEDS1 homodimer constructed by superimposition of two AtEDS1 monomers from PDB_ID 4NFU (Wagner et al., 2013) on the VvEDS1^{Nterm} dimer in panel (d). (f–h) Homodimer models of VvEDS1$^{1-331}$, which is the structurally well-defined part of VvEDS1^{Nterm} (f), of the complete VvEDS1^{Nterm} protein (g), and of full-length VvEDS1 (h) calculated with AlphaFold-Multimer (Evans et al., 2022). The figure was prepared with PyMOL (PyMOL, 2013).

1469896x, 2023, 4, Downloaded from https://onlinelibrary.wiley.com/doi/10.1002/pro.4624 by Bibl. der Universitat zu Koln, Wiley Online Library on [23/11/2026]. See the Terms and Conditions (https://onlinelibrary.wiley.com/terms-and-conditions) on Wiley Online Library for rules of use; OA articles are governed by the applicable Creative Commons License

additional strands (β9 and β10) with two supplementary helices (αI and αJ) in their interconnection; (iii) finally, the helical insert αF, αG, and αH, a functional key region of AtEDS1 because αG and αH contribute to the interface either to AtPAD4 or to AtSAG101 (Wagner et al., 2013), is fully established. Remarkably, the prominent interaction helix αH of VvEDS1^{Nterm} has a different orientation and is shorter than its counterpart in AtSAG101-bound AtEDS1 (Figure 3b); it also appears to be more rigid than the latter, supported by a hydrogen bond of its final residue Arg252, which has no equivalent in AtEDS1 (Figure 1), to the carbonyl group of Thr255 (Figure 3b). These differences are probably among the reasons why VvEDS1 can interact with VvPAD4 and AtPAD4, but AtEDS1 only with the latter (Gao et al., 2014).

Similar to AtEDS1, no funnel leads to the catalytic serine (Ser123). Shielded by Trp51 and the helix αF (Figure 3c), it is inaccessible for potential substrates in the observed conformation of VvEDS1^{Nterm}. Yet, with the view to the possibility of a hidden catalytic activity of EDS1—which was given new impetus by a recent report that mutations in the SHD triad of tomato EDS1 lead to significant phenotypes in certain immunity assays performed in a *Nicotiana benthamiana* model system (Zönnchen et al., 2022)—two differences to AtEDS1 are noteworthy: first, in VvEDS1^{Nterm}, more space is available next to Ser123 than in AtEDS1 where it is restricted by the Phe47 side chain (Figure 3c); this is visible from an overlay of a lipase with a diethyl phosphonate adduct to mimic the reaction transition state (Derewenda et al., 1992) (Figure 3c) and from a second bound water molecule (Wat2 in Figure 3c) not present in any of the seven published AtEDS1 structures (Huang et al., 2022; Jia et al., 2022; Voss et al., 2019; Wagner et al., 2013). Second, in VvEDS1, the residue following Ser123 is a tryptophan (Trp124, Figure 3c) rather than a serine as in AtEDS1 (Figure 1b) and in the majority of known EDS1 sequences; this means that in VvEDS1 the potential oxyanion hole required for hydrolytic activity is not partially blocked by a hydrogen bond to the Ser124 side chain as described for AtEDS1 (Voss et al., 2019; Wagner et al., 2013).

We analyzed then the crystalline neighborhood of VvEDS1^{Nterm} computationally with PISA (Krissinel & Henrick, 2007) and EPPIC (Bliven et al., 2018). Both programs came to the result that VvEDS1^{Nterm} forms stable homodimers in solution as visible in Figure 3d. In particular, the protein/protein interface of nearly 1400 Å^2 is typical for homodimers of this size (Jones & Thornton, 1996), but also other parameters reported to be relevant for such an assessment (Jones & Thornton, 1996) like the mean hydrophobicity (0.06, according to the scale of Janin et al., 1988) or the number of hydrogen bonds across the interface (6, meaning 0.43 hydrogen bonds per 100 Å^2 interface area) are in favor of a homodimeric quaternary structure. Two of these hydrogen bonds alone are formed by Tyr290, a particularly striking interface residue and potential homodimerization hotspot (Figure 3b). In summary, the computational analysis of the crystal packing fits well to the gel filtration result of VvEDS1^{Nterm} in solution (Figure 2).

The interface that constitutes the VvEDS1^{Nterm} dimer is formed by the helices αG, αH, and αI (Figure 3d). In AtEDS1, the equivalents of αG and αH contribute to the AtEDS1/AtSAG101 interface (Wagner et al., 2013). In particular the protruding helix αH (Figure 3a) is a key element for heterodimerization. It has no pendant in AtSAG101 so that in the AtEDS1/AtSAG101 complex, no helix bundle interface similar to Figure 3d is possible; rather, αH of AtEDS1 is harbored by a shallow groove located near the N-terminus of AtSAG101 so that the two α/β-hydrolase fold scaffolds of AtEDS1 and AtSAG101 are arranged in an asymmetric way in stark contrast to what is typical for homodimers (Voss et al., 2019). Hydrophobic residues on the surface of αH serve as heterodimerization hot spots; the collective removal of their side chains by site-directed mutagenesis leads to an AtEDS1 mutant unable to interact with AtSAG101 or AtPAD4 and to compensate knocked out AtEDS1 *in planta* in infection assays (Wagner et al., 2013). Assuming that αG and αH have a similar heterodimerization function in VvEDS1, their occupation for homodimerization in VvEDS1^{Nterm} directly explains our observation from gel filtration (Figure 2) that VvEDS1^{Nterm} is unable to interact with VvPAD4.

2.4 | Inferences about the homodimerization of full-length EDS1

Can full-length EDS1 dimerize via the same interface as VvEDS1^{Nterm}? Although AtEDS1 in the absence of AtSAG101 or AtPAD4 was found as a monomer in solution and in crystals (Voss et al., 2019), this question is still relevant because of earlier reports about its ability to self-interact (Feys et al., 2001; Gao et al., 2014; Wagner et al., 2013) and homodimerize (Rietz et al., 2011). Also for VvEDS1, self-interaction was observed (Gao et al., 2014). Therefore, we superimposed two AtEDS1 monomers on both chains of the VvEDS1^{Nterm} dimer in Figure 3d. In the resulting model, the EP domains give way to each other, but there are serious steric conflicts at the N-terminal domains (Figure 3e). The helices αG and αH clash with αL and αM, two helices of the full-length protein, which lie entirely or partially within the disordered C-terminal region of VvEDS1^{Nterm}. Since structural

1469896x, 2023, 4, Downloaded from https://onlinelibrary.wiley.com/doi/10.1002/pro.4624 by Bibl. der Universitat zu Koln, Wiley Online Library on [23/11/2026]. See the Terms and Conditions (https://onlinelibrary.wiley.com/terms-and-conditions) on Wiley Online Library for rules of use; OA articles are governed by the applicable Creative Commons License

studies with monomeric AtEDS1 revealed the propensity of αH to unfold and to lose its helical conformation (Voss et al., 2019), a release of the αL/αH clash in Figure 3e is conceivable, but a comparable plasticity is unknown for EDS1's long helices αG and αM. Therefore, their overlap in Figure 3e is the main argument that the VvEDS1^{Nterm} dimer of Figure 3d does not directly represent a model of potential full-length EDS1 dimers.

Nevertheless, the experimental VvEDS1^{Nterm} dimer can serve as a guide to evaluate homodimer models of EDS1 constructs calculated with AlphaFold-Multimer (Evans et al., 2022). To test the method, we generated such models with VvEDS1$^{1-331}$, which comprises all VvEDS1^{Nterm} residues visible in the electron density, and with the complete VvEDS1^{Nterm} protein (Figure 1). 3D-fits of the resulting *in silico* homodimers (Figure 3f,g) on the x-ray structure (Figure 3d) led to RMS deviations of 2.3 Å for VvEDS1$^{1-331}$ and of 4.9 Å for VvEDS1^{Nterm}/complete with both values refering to 656 of 662 possible C_α-atoms. This computational similarity of the calculated and the experimentally determined homodimers matches the visual impression when comparing Figure 3f,g with Figure 3d. It demonstrates the power of the approach, which is all the more remarkable as no experimental structural information on EDS1 homodimers is currently publicly available.

This success confers a certain degree of reliability to an *in silico* homodimer model of full-length VvEDS1 calculated with AlphaFold-Multimer (Evans et al., 2022) (Figure 3h). In this case, a 3D-fit on the VvEDS1^{Nterm} crystal structure results in a high RMS deviation of 11.4 Å for 656 C_α-atoms; nevertheless, the overall arrangement of the N-terminal domains of VvEDS1 and the involvement of the helices αG and αH in the dimerization interface resembles the experimental VvEDS1$^{N\text{-}term}$ dimer (Figure 3d). In the homodimer model of full-length VvEDS1, the EP domains do not contribute to the interface (Figure 3h). With only 731 Å^2, its size is consistent with a nonpermanent protein/protein interaction (Jones & Thornton, 1996). Subject to their experimental verification, such transient EDS1 homodimers in *V. vinifera* or other plant species would make physiological sense: they could serve as a pool to provide monomers for the formation of EDS1/PAD4 or EDS1/SAG101 heterodimers, the actual functional units in EDS1-dependent immunity signaling in plants.

3 | CONCLUSION

The existing structural knowledge of EDS1 (Huang et al., 2022; Jia et al., 2022; Voss et al., 2019; Wagner et al., 2013) is supplemented here by the crystal structure of VvEDS1^{Nterm}, the first structure of an EDS1 entity beyond *A. thaliana*. VvEDS1^{Nterm} forms stable homodimers, which exclude the formation of heterodimers with VvPAD4. These VvEDS1^{Nterm} homodimers contribute to the development of a plausible, albeit experimentally unconfirmed, model for full-length EDS1 homodimers. VvEDS1^{Nterm} is encoded by an mRNA from a natural source retaining the last intron of the *VvEDS1* gene. This is the first report of potential intron retention in the context of EDS1; its potential physiological role remains to be clarified.

4 | MATERIALS AND METHODS

4.1 | RNA/cDNA sequence analysis

V. vinifera "Cabernet Sauvignon" leaf material was flash frozen in liquid nitrogen and stored at −80°C. For isolation of *VvEDS1* cDNA clones and splice variants, total RNA was extracted using a rapid CTAB approach developed for grapevine (Gambino et al., 2008). Total RNA samples were treated with TURBO DNase (Invitrogen) following the manufacturer's recommendations. Purified mRNA was then isolated from 5 μg of DNA-free RNA using the NEBNext Poly(A) mRNA Magnetic Isolation Module (NEB). First strand cDNA synthesis was completed using M-MLV Reverse Transcriptase (Promega), and full-length RT-PCR products were amplified using primers specific to the entire coding region of *VvEDS1* (Gao et al., 2010) and Phusion High-fidelity Polymerase (Thermo Fisher Scientific) with the following PCR conditions: 98°C, 2 min; 35 cycles of 98°C, 10 s; 60°C, 30 s; 72°C, 45 s, with final extension 72°C for 5 min. PCR products were A-tailed and cloned into pGEMT-Easy (Promega). Clones were prescreened with diagnostic restriction digests and sequenced, confirming retention of intron 1 or intron 2, with the other intron spliced out, in individual cDNAs.

qRT-PCR was performed to quantify the levels of alternative splicing using primer sets specific to each intron, with a similarly sized amplicon located between the two introns for overall *VvEDS1* mRNA quantitation. qRT-PCR was performed as described by Spears et al. (2019) with 5 μL of 20× diluted cDNA and a primer concentration of 1 μM in 20-μL reactions with Brilliant III Ultra-Fast SYBR GREEN master mix (Agilent Technologies) run on a Bio-Rad CFX Connect thermocycler (Bio-Rad). qRT-PCR conditions were as follows: 95°C, 10 min; 40 cycles of 95°C, 10 s; 60°C, 60 s; finishing with a melt curve from 60°C to 95°C. Reactions without added RT were used to control for DNA contamination. qRT-PCR end point reactions were also sequenced as above,

1469896x, 2023, 4, Downloaded from https://onlinelibrary.wiley.com/doi/10.1002/pro.4624 by Bibl. der Universitat zu Koln, Wiley Online Library on [23/11/2026]. See the Terms and Conditions (https://onlinelibrary.wiley.com/terms-and-conditions) on Wiley Online Library for rules of use; OA articles are governed by the applicable Creative Commons License

confirming that intron 2 is retained in the cDNA pool. Transcript levels of target were calculated using the ΔC_T method, indicating that ~4% of transcripts retained intron 1 and ~8% retained intron 2.

4.2 | Protein expression and purification

To prepare VvPAD4 and VvEDS1^{Nterm} and to supply them with an N-terminal $(His)_6$-tag, their genes were cloned into a pETM11 vector. For bacterial expression, the *Escherichia coli* strain Rosetta(DE3)pLysS from Novagen was used in both cases. The bacteria were grown at 37°C in lysogeny broth-medium (10 g/L tryptone, 5 g/L yeast extract, 10 g/L NaCl) containing 50 μg/mL kanamycin, until an OD_{600} value of 0.6 was reached. The gene expression was induced by the addition of 0.5 mM isopropyl-thiogalactopyranoside and was performed overnight at 18°C. The cells were harvested by centrifugation (3300 × *g*) at 4°C, washed, stored at −80°C and later resuspended in a lysis/wash buffer (300 mM NaCl, 10% glycerol, 20 mM imidazole, 1 mM DTT, 50 mM HEPES, pH 8) enriched with 0.8 mg/mL lysozyme, 10 μg/mL DNase I, and 0.05% Triton-X100. The cells were incubated for 60 min on ice and sonicated afterwards. Cell debris was removed by centrifugation (20,000 × *g*, 45 min, 4°C).

For purification by metal chelate affinity chromatography, each supernatant of a centrifugation was applied to a 1-mL NiNTA agarose cartridge (Cube Biotech) previously equilibrated with lysis/wash buffer. After washing with 20 mL lysis/wash buffer, the $(His)_6$-tagged target protein (VvPAD4 or VvEDS1^{Nterm}) was eluted with an imidazole gradient using 300 mM NaCl, 10% glycerol, 250 mM imidazole, 1 mM DTT, 50 mM HEPES, pH 8, as high-concentration solution and afterwards concentrated by ultrafiltration.

As a second chromatographic purification step, size exclusion chromatography (gel filtration) was performed using a HiLoad Superdex 200 16/60 column (GE Healthcase). The equilibration and running buffer for the gel filtration column was 300 mM NaCl, 1% (vol/-vol) glycerol, 1 mM DTT, 50 mM HEPES, pH 8.0. Finally, the proteins were concentrated by ultrafiltration.

4.3 | Analytical gel filtration analysis

To estimate the native molecular weight of VvPAD4, VvEDS1^{Nterm} and of an equimolar mixture of both and to determine the oligomeric states of these samples, analytical gel filtration chromatography was performed using a Superdex 200 10/300Gl column (GE Healthcare) equilibrated in 300 mM NaCl, 1% (vol/vol) glycerol, 1 mM DTT, 50 mM HEPES, pH 8.0. A volume of 500 μL concentrated protein sample was applied. The column was calibrated with four standard proteins of different size (lysozyme: 14.3 kDa; bovine serum albumin: 66.4 kDa; lactate dehydrogenase: 140 kDa; ferritin: 474 kDa).

4.4 | Differential scanning fluorimetry (ThermoFluor)

As a preparation for crystallization, VvEDS1^{Nterm} and VvPAD4 were thermostabilized by optimization of their solution environments via differential scanning fluorimetry (ThermoFluor). ThermoFluor screens were performed using a protocol based on the approach of Boivin et al. (2013). Typically to each well of a screening plate, 21 μL of the respective buffer to be tested was pipetted together with 2 μL 25 μM highly purified protein in gel filtration buffer. Three microliters of a commercial stock solution of Sypro-orange dye in dimethyl sulfoxide (Thermo Fisher Scientifc) was diluted with 237 μL water; 2 μL of this mixture was added to the solution in each well of the screening plate. After sealing the plate and careful mixing by gentle centrifugation, melting curves were recorded in a CFX96 real-time PCR machine (Bio-Rad). The temperature was increased from 4°C to 96°C in steps of 0.5°C per 30 s. The fluorescence of the Sypro-orange dye was recorded before each heating step. The results were analyzed with the CFX Manager software (Bio-Rad) providing melting curves and melting temperatures. For each protein, we determined optimal buffer and pH conditions in a first ThermoFluor screen while in a second run, different salts and additives were tested to further increase the thermal stability. The resulting final solution for VvEDS1^{Nterm} and VvPAD4 was 300 mM sodium iodide, 1% (vol/vol) glycerol, 1 mM DTT, 50 mM HEPES, pH 8.0.

4.5 | Crystallization and structure determination

The sitting-drop variant of the vapor diffusion method was applied for all protein crystallization experiments. The protein solution—either VvPAD4 or VvEDS1^{Nterm}—contained 4.5 mg/mL protein in 300 mM sodium iodide, 1% (vol/vol) glycerol, 1 mM DTT, 50 mM HEPES, pH 8.0. Several commercial crystallization screens were tested; they were unsuccessful for VvPAD4, but VvEDS1^{Nterm} crystallized under a broad range of conditions containing mostly 25% (wt/vol) PEG3350, 0.2 M of different sodium

1469896x, 2023, 4, Downloaded from https://onlinelibrary.wiley.com/doi/10.1002/pro.4624 by Bibl. der Universitat zu Koln, Wiley Online Library on [23/11/2026]. See the Terms and Conditions (https://onlinelibrary.wiley.com/terms-and-conditions) on Wiley Online Library for rules of use; OA articles are governed by the applicable Creative Commons License

salts (sulfate, citrate, nitrate, iodide, bromide, fluoride, tartrate, and malate) with a pH value between 6.5 and 8.5. The optimal vapor diffusion reservoir solution—mixed in a 1:1 volume ratio with the protein solution in the crystallization drop—was 12% (wt/vol) PEG3350, 0.3 M cesium chloride, 100 mM Bis-Tris buffer, pH 8.5.

The VvEDS1^{Nterm} crystals were cryo-protected in their mother liquor plus 30% (vol/vol) ethylene glycol and then flash frozen in liquid nitrogen. X-ray diffraction data were collected at beamline ID30B of the European Synchrotron Radiation Facility (ESRF) in Grenoble, France. The diffraction data (Table 1) were processed with the AUTOPROC toolbox (version 1.0.5) (Vonrhein et al., 2011) which comprised XDS (Kabsch, 2010) for indexing and integration, POINTLESS (Evans, 2006), and AIMLESS (Evans & Murshudov, 2013) from the CCP4 suite (Winn et al., 2011) for space group determination and scaling as well as STARANISO (Tickle et al., 2018) for anisotropy analysis.

The VvEDS1^{Nterm} structure was solved with molecular replacement using PHASER (McCoy et al., 2007) within PHENIX (Adams et al., 2010). The N-terminal domain of *At*EDS1 in PDB entry 4NFU (Wagner et al., 2013) served as search model. The structure was optimized to high quality (Table 1) with several rounds of PHENIX auto building (Terwilliger et al., 2008) and refinement (Adams et al., 2010) alternating with manual modeling with COOT (Emsley et al., 2010).

4.6 | Computational analyses

To analyze the protein interfaces and assemblies within the VvEDS1^{Nterm} crystal packing, the final VvEDS1^{Nterm} crystal structure (Table 1) was uploaded to the PISA server (https://www.ebi.ac.uk/pdbe/pisa/) (Krissinel & Henrick, 2007) and to the EPPIC site (https://www.eppic-web.org/ewui/) (Bliven et al., 2018). Homodimer models of VvEDS1 constructs were predicted with AlphaFold-Multimer (Evans et al., 2022) as implemented in the Cosmic2 gateway (https://cosmic2.sdsc.edu) (Cianfrocco et al., 2017); in each case, the model with the highest score was selected for representation (Figure 3f–h). 3D-fits and RMS deviations were calculated with the Align function of PyMOL (PyMOL, 2013) and were restricted to the C_α-atoms. For the evaluation of the AlphaFold-Multimer homodimer models in Figure 3f–h, the cut-off distance to detect equivalent C_α-atoms was increased to 5 Å.

AUTHOR CONTRIBUTIONS

Martin Voss: Conceptualization (equal); investigation (lead); writing – original draft (supporting); writing – review and editing (equal). **Leland J. Cseke:** Conceptualization (equal); investigation (supporting); writing – original draft (supporting); writing – review and editing (supporting). **Walter Gassmann:** Conceptualization (equal); writing – original draft (supporting); writing – review and editing (equal). **Karsten Niefind:** Conceptualization (equal); funding acquisition (lead); writing – original draft (lead); writing – review and editing (equal).

ACKNOWLEDGMENTS

The authors thank the staff of the ESRF—in particular at beamline ID30B—for assistance with x-ray diffraction data collection and Prof. Ulrich Baumann (University of Cologne) for access to protein crystallography infrastructure (c2f.uni-koeln.de), Drs. Lance Cadle-Davidson and Surya Datta Sapkota, USDA-ARS Grape Genetics Research Unit and Cornell University, NY, for providing us with *V. vinifera* "Cabernet Sauvignon" leaf tissue, and the University of Missouri Genomics Technology Core for DNA sequencing services. The work was funded by the Deutsche Forschungsgemeinschaft (DFG; grant NI 643/6-1). Open Access funding enabled and organized by Projekt DEAL.

CONFLICT OF INTEREST STATEMENT

The authors declare no conflict of interest.

DATA AVAILABILITY STATEMENT

The 3D coordinates and structure factors for VvEDS1^{Nterm} are available at the RCSB Protein Data Bank under accession code 8B28. All other data are available upon request.

ORCID

Leland J. Cseke https://orcid.org/0000-0003-1746-6600
Walter Gassmann https://orcid.org/0000-0002-7527-0385
Karsten Niefind https://orcid.org/0000-0002-0183-6315

REFERENCES

Adams PD, Afonine PV, Bunkóczi G, Chen VB, Davis IW, Echols N, et al. PHENIX: a comprehensive python-based system for macromolecular structure solution. Acta Crystallogr D Biol Crystallogr. 2010;66:213–21.

Bliven S, Lafita A, Parker A, Capitani G, Duarte JM. Automated evaluation of quaternary structures from protein crystals. PLoS Comput Biol. 2018;14:e1006104.

Boivin S, Kozak S, Meijers R. Optimization of protein purification and characterization using thermofluor screens. Protein Expr Purif. 2013;91:192–206.

Brown GR, Hem V, Katz KS, Ovetsky M, Wallin C, Ermolaeva O, et al. Gene: a gene-centered information resource at NCBI. Nucleic Acids Res. 2015;43:D36–42.

1469896x, 2023, 4, Downloaded from https://onlinelibrary.wiley.com/doi/10.1002/pro.4624 by Bibl. der Universitat zu Koln, Wiley Online Library on [23/11/2026]. See the Terms and Conditions (https://onlinelibrary.wiley.com/terms-and-conditions) on Wiley Online Library for rules of use; OA articles are governed by the applicable Creative Commons License

Chaudhary S, Jabre I, Reddy ASN, Staiger D, Syed NH. Perspective on alternative splicing and proteome complexity in plants. Trends Plant Sci. 2019;24:496–506.

Chong J, Le Henanff G, Bertsch C, Walter B. Identification, expression analysis and characterization of defense and signaling genes in *Vitis vinifera*. Plant Physiol Biochem. 2008;46:469–81.

Cianfrocco MA, Wong-Barnum M, Youn C, Wagner R, Leschziner A. COSMIC2: a science gateway for cryo-electron microscopy structure determination. Proceedings of the Practice and Experience in Advanced Research Computing 2017 on Sustainability, Success and Impact. New Orleans, LA: Association for Computing Machinery. 2017 https://doi.org/10.1145/3093338.3093390

Derewenda U, Brzozowski AM, Lawson DM, Derewenda ZS. Catalysis at the interface: the anatomy of a conformational change in a triglyceride lipase. Biochemistry. 1992;31:1532–41.

Emsley P, Lohkamp B, Scott WG, Cowtan K. Features and development of coot. Acta Crystallogr D Biol Crystallogr. 2010;66:486–501.

Evans P. Scaling and assessment of data quality. Acta Crystallogr D Biol Crystallogr. 2006;62:72–82.

Evans PR, Murshudov GN. How good are my data and what is the resolution? Acta Crystallogr D Biol Crystallogr. 2013;69:1204–14.

Evans R, O'Neill M, Pritzel A, Antropova N, Senior A, Green T, et al. Protein complex prediction with AlphaFold-Multimer. bioRxiv. 2022. https://doi.org/10.1101/2021.10.04.463034

Falk A, Feys BJ, Frost LN, Jones JD, Daniels MJ, Parker JE. *EDS1*, an essential component of *R* gene-mediated disease resistance in *Arabidopsis* has homology to eukaryotic lipases. Proc Natl Acad Sci U S A. 1999;96:3292–7.

Feys BJ, Moisan LJ, Newman MA, Parker JE. Direct interaction between the *Arabidopsis* disease resistance signaling proteins, EDS1 and PAD4. EMBO J. 2001;20:5400–11.

Feys BJ, Wiermer M, Bhat RA, Moisan LJ, Medina-Escobar N, Neu C, et al. *Arabidopsis* SENESCENCE-ASSOCIATED $GENE_{101}$ stabilizes and signals within an ENHANCED DISEASE $SUSCEPTIBILITY_1$ complex in plant innate immunity. Plant Cell. 2005;17:2601–13.

Fung RW, Gonzalo M, Fekete C, Kovacs LG, He Y, Marsh E, et al. Powdery mildew induces defense-oriented reprogramming of the transcriptome in a susceptible but not in a resistant grapevine. Plant Physiol. 2008;146:236–49.

Gambino G, Perrone I, Gribaudo I. A rapid and effective method for RNA extraction from different tissues of grapevine and other woody plants. Phytochem Anal. 2008;19:520–5.

Gao F, Dai R, Pike SM, Qiu WP, Gassmann W. Functions of *EDS1*-*like* and *PAD4* genes in grapevine defenses against powdery mildew. Plant Mol Biol. 2014;86:381–93.

Gao F, Shu X, Ali MB, Howard S, Li N, Winterhagen P, et al. A functional *EDS1* ortholog is differentially regulated in powdery mildew resistant and susceptible grapevines and complements an Arabidopsis *eds1* mutant. Planta. 2010;231:1037–47.

Gloggnitzer J, Akimcheva S, Srinivasan A, Kusenda B, Riehs N, Stampfl H, et al. Nonsense-mediated mRNA decay modulates immune receptor levels to regulate plant antibacterial defense. Cell Host Microbe. 2014;16:376–90.

He Y, Gan S. A gene encoding an acyl hydrolase is involved in leaf senescence in Arabidopsis. Plant Cell. 2002;14:805–15.

Huang S, Jia A, Song W, Hessler G, Meng Y, Sun Y, et al. Identification and receptor mechanism of TIR-catalyzed small molecules in plant immunity. Science. 2022;377:eabq3297.

Janin J, Miller S, Chothia C. Surface, subunit interfaces and interior of oligomeric proteins. J Mol Biol. 1988;204:155–64.

Jia A, Huang S, Song W, Wang J, Meng Y, Sun Y, et al. TIR-catalyzed ADP-ribosylation reactions produce signaling molecules for plant immunity. Science. 2022;377:eabq8180.

Jirage D, Tootle TL, Reuber TL, Frost LN, Feys BJ, Parker JE, et al. *Arabidopsis thaliana* PAD4 encodes a lipase-like gene that is important for salicylic acid signaling. Proc Natl Acad Sci U S A. 1999;96:13583–8.

Jones S, Thornton JM. Principles of protein-protein interactions. Proc Natl Acad Sci U S A. 1996;93:13–20.

Kabsch W. XDS. Acta Crystallogr D Biol Crystallogr. 2010;66:125–32.

Kalyna M, Simpson CG, Syed NH, Lewandowska D, Marquez Y, Kusenda B, et al. Alternative splicing and nonsense-mediated decay modulate expression of important regulatory genes in Arabidopsis. Nucleic Acids Res. 2012;40:2454–69.

Krissinel E, Henrick K. Inference of macromolecular assemblies from crystalline state. J Mol Biol. 2007;372:774–97.

Kufel J, Diachenko N, Golisz A. Alternative splicing as a key player in the fine-tuning of the immunity response in Arabidopsis. Mol Plant Pathol. 2022;23:1226–38.

Lykke-Andersen S, Jensen TH. Nonsense-mediated mRNA decay: an intricate machinery that shapes transcriptomes. Nat Rev Mol Cell Biol. 2015;16:665–77.

Magris G, Jurman I, Fornasiero A, Paparelli E, Schwope R, Marroni F, et al. The genomes of 204 *Vitis vinifera* accessions reveal the origin of European wine grapes. Nat Commun. 2021;12:7240.

McCoy AJ, Grosse-Kunstleve RW, Adams PD, Winn MD, Storoni LC, Read RJ. Phaser crystallographic software. J Appl Cryst. 2007;40:658–74.

Mistry J, Chuguransky S, Williams L, Qureshi M, Salazar GA, Sonnhammer ELL, et al. Pfam: the protein families database in 2021. Nucleic Acids Res. 2021;49:D412–9.

Ollis DL, Cheah E, Cygler M, Dijkstra B, Frolow F, Franken SM, et al. The α/β hydrolase fold. Protein Eng. 1992;5:197–211.

Parker JE, Holub EB, Frost LN, Falk A, Gunn ND, Daniels MJ. Characterization of *eds1*, a mutation in Arabidopsis suppressing resistance to *Peronospora parasitica* specified by several different RPP genes. Plant Cell. 1996;8:2033–46.

Pruitt RN, Locci F, Wanke F, Zhang L, Saile SC, Joe A, et al. The EDS1–PAD4–ADR1 node mediates *Arabidopsis* pattern-triggered immunity. Nature. 2021;598:495–9.

PyMOL. The PyMOL molecular graphics system. 1.7 ed: Schrödinger, LLC. 2013.

Qiu W, Feechan A, Dry I. Current understanding of grapevine defense mechanisms against the biotrophic fungus (*Erysiphe necator*), the causal agent of powdery mildew disease. Hortic Res. 2015;2:15020.

Rietz S, Stamm A, Malonek S, Wagner S, Becker D, Medina-Escobar N, et al. Different roles of enhanced disease susceptibility1 (EDS1) bound to and dissociated from phytoalexin deficient 4 (PAD4) in Arabidopsis immunity. New Phytol. 2011;191:107–19.

1469896x, 2023, 4, Downloaded from https://onlinelibrary.wiley.com/doi/10.1002/pro.4624 by Bibl. der Universitat zu Koln, Wiley Online Library on [23/11/2026]. See the Terms and Conditions (https://onlinelibrary.wiley.com/terms-and-conditions) on Wiley Online Library for rules of use; OA articles are governed by the applicable Creative Commons License

Sayers EW, Cavanaugh M, Clark K, Pruitt KD, Schoch CL, Sherry ST, et al. GenBank. Nucleic Acids Res. 2022;50:D161–4.

Spears BJ, Howton TC, Gao F, Garner CM, Mukhtar MS, Gassmann W. Direct regulation of the *EFR*-dependent immune response by *Arabidopsis* TCP transcription factors. Mol Plant Microbe Interact. 2019;32:540–9.

Sun X, Lapin D, Feehan JM, Stolze SC, Kramer K, Dongus JA, et al. Pathogen effector recognition-dependent association of NRG1 with EDS1 and SAG101 in TNL receptor immunity. Nat Commun. 2021;12:3335.

Terwilliger TC, Grosse-Kunstleve RW, Afonine PV, Moriarty NW, Zwart PH, Hung LW, et al. Iterative model building, structure refinement and density modification with the PHENIX AutoBuild wizard. Acta Crystallogr D Biol Crystallogr. 2008;64:61–9.

Tickle IJ, Flensburg C, Keller P, Paciorek W, Sharff A, Vonrhein C, et al. STARANISO. Cambridge, UK: Global Phasing Ltd.; 2018.

UniProt Consortium. UniProt: the universal protein knowledgebase in 2021. Nucleic Acids Res. 2021;49:D480–9.

Vonrhein C, Flensburg C, Keller P, Sharff A, Smart O, Paciorek W, et al. Data processing and analysis with the autoPROC toolbox. Acta Crystallogr D Biol Crystallogr. 2011;67:293–302.

Voss M, Toelzer C, Bhandari DD, Parker JE, Niefind K. *Arabidopsis* immunity regulator EDS1 in a PAD4/SAG101-unbound form is a monomer with an inherently inactive conformation. J Struct Biol. 2019;208:107390.

Wagner S. Analysing novel structures of protein complexes requiring the central plant immune regulator EDS1. PhD thesis. Cologne, Germany: Universität zu Köln. 2013 Available from: https://kups.ub.uni-koeln.de/5341/

Wagner S, Stuttmann J, Rietz S, Guerois R, Brunstein E, Bautor J, et al. Structural basis for signaling by exclusive EDS1 heteromeric complexes with SAG101 or PAD4 in plant innate immunity. Cell Host Microbe. 2013;14:619–30.

Wiermer M, Feys BJ, Parker JE. Plant immunity: the EDS1 regulatory node. Curr Opin Plant Biol. 2005;8:383–9.

Winn MD, Ballard CC, Cowtan KD, Dodson EJ, Emsley P, Evans PR, et al. Overview of the *CCP4* suite and current developments. Acta Crystallogr D Biol Crystallogr. 2011;67:235–42.

Wong JJ, Schmitz U. Intron retention: importance, challenges, and opportunities. Trends Genet. 2022;38:789–92.

Zhang Y, Skolnick J. TM-align: a protein structure alignment algorithm based on the TM-score. Nucleic Acids Res. 2005;33:2302–9.

Zönnchen J, Gantner J, Lapin D, Barthel K, Eschen-Lippold L, Erickson JL, et al. EDS1 complexes are not required for PRR responses and execute TNL-ETI from the nucleus in *Nicotiana benthamiana*. New Phytol. 2022;236:2249–64.

How to cite this article: Voss M, Cseke LJ, Gassmann W, Niefind K. A splicing variant of EDS1 from *Vitis vinifera* forms homodimers but no heterodimers with PAD4. Protein Science. 2023; 32(4):e4624. https://doi.org/10.1002/pro.4624

1469896x, 2023, 4, Downloaded from https://onlinelibrary.wiley.com/doi/10.1002/pro.4624 by Bibl. der Universitat zu Koln, Wiley Online Library on [23/11/2026]. See the Terms and Conditions (https://onlinelibrary.wiley.com/terms-and-conditions) on Wiley Online Library for rules of use; OA articles are governed by the applicable Creative Commons License